A NEW MODEL FOR HADRONIC INTERACTIONS AT INTERMEDIATE ENERGIES FOR THE FLUKA CODE

A. FERRARI and P.R. SALA
I.N.F.N., sez. di Milano, via Celoria 16
Milano, 20133, Italy

ABSTRACT

A new algorithm combining intranuclear cascade and exciton models has been developed for the FLUKA code. The algorithm is presently applicable to nucleon and pion induced reactions below 300 MeV. An extension to 1 GeV is planned. Comparisons with experimental data are presented.

1. Introduction

The FLUKA code[1,2] has been successfully used for years to simulate showers initiated by high energy hadrons, both for targetry and shielding purposes. The call for a more accurate simulation of intermediate and low energy interactions arose, somehow paradoxically, from the first radiation studies for LHC and SSC. The high luminosity and energy of these machines strongly amplify problems which were previously considered negligible or easily manageable, such as radiation damage to electronic devices, activation of irradiated materials, pile-up in the detectors due to background events, and radiation hazard in counting rooms. Any calculation aiming to give reliable predictions on these, and other, items, must be able to cope successfully with the production and transport of low energy particles (thermal neutrons are perhaps the best example), and with showers initiated by minimum-bias particles. The intermediate energy event generator implemented in FLUKA87[3] consisted of the production and decay of one or more resonances coupled to a parametrized nuclear cascade. Despite many improvements in the parametrizations, in the kinematics and in the treatment of nuclear effects,[2,5,6] it became increasingly inaccurate at energies lower than about 1 GeV. Moreover, the hadronic transport cutoff in FLUKA87 was set at 50 MeV, too high even for the coupling with the newly implemented neutron transport algorithm,[5] which can be applied only below 20 MeV.

Indeed, a correct treatment of the nuclear thermalization process including a preequilibrium stage is still missing in most MonteCarlo codes, except LAHET which includes a specialized algorithm.[4]

The algorithm described here, called PEANUT (for PreEquilibrium Approach to NUclear Thermalization) is intended to eventually handle interactions of nucleons, pions and α particles with nuclei from about 1 GeV down to reaction threshold (or 20 MeV for neutrons). It is not yet complete, in the sense that up to now the higher limit is about 300 MeV and pion interactions are treated in a

preliminary way.

2. Models for Preequilibrium reactions

The intranuclear cascade model[7] (INC) is the most straightforward approach when writing a MonteCarlo code, and has been successfully used for decades in the intermediate energy region. However, its physical foundation becomes approximate at low energies,[8] resulting in a decrease of its accuracy. Moreover, it can be very time consuming, since many particles must be followed down to very low energies.

On the other hand, a description based simply on direct reaction plus compound nucleus evaporation is surely not sufficient. Already in 1966 Griffin[9] described the spectra following nucleon-induced reactions in terms of a "preequilibrium" model, that is, a transition between the first step of the reaction and the final thermalization.

Since then, many models have been developed (see[8] for an exhaustive review). The two leading approaches (with many different implementations) are the quantum-mechanical multistep model,[10] which has a very good theoretical background, but is complex and poses some difficulties to the description of multiple nucleon emission, and the exciton model,[9,8,11] which relies on statistical assumptions. This makes it very simple and fast, but of course leads to some limitations, especially for medium-high energy projectiles.

The solution adopted in PEANUT tries to be a compromise between accuracy and speed, being a combination of exciton model and intranuclear cascade.

3. Description of the algorithm

3.1 Implementation of the exciton model

The approach followed here is that formalized by M.Blann and coworkers[12,13] called Geometry Dependent Hybrid Model (GDH), with some slight modifications. We list here only the modifications, as the model is well described in the original papers.

The rate of exciton emission (λ_c in[12]) is related to the cross section of the inverse process (σ_{inv}). The values of σ_{inv} adopted in PEANUT are obtained with energy and Z dependent fits to experimental data. This approach gives better results than the normally used Dostrowsky expressions,[14] which are energy independent except near threshold. The exciton reinteraction rate (λ_+ in[12]) is calculated using a fit to experimental nucleon-nucleon cross sections corrected for Fermi motion and Pauli principle with the factor given by Kikuchi and Kawai.[15]

An approximate treatment of discrete energy levels of residual nuclei has been implemented. The first (and sometimes also the second) excited level has been tabulated for some low-mass and near-magic nuclei, while for the others the first level is assumed to correspond to an excitation energy equal to the pairing gap for the nucleon type concerned. At emission stage, if the excitation energy of the

residual nucleus lies in between two discrete levels (ground or excited), it is forced to coincide with the nearest one. The same is applied in the INC part of the code.

This model works very nicely for low energy projectiles, but has some well known problems at higher energies, where it tends to underestimate the emission of fast particles and cannot be applied to pion-nucleus interactions other than stopped pion capture.

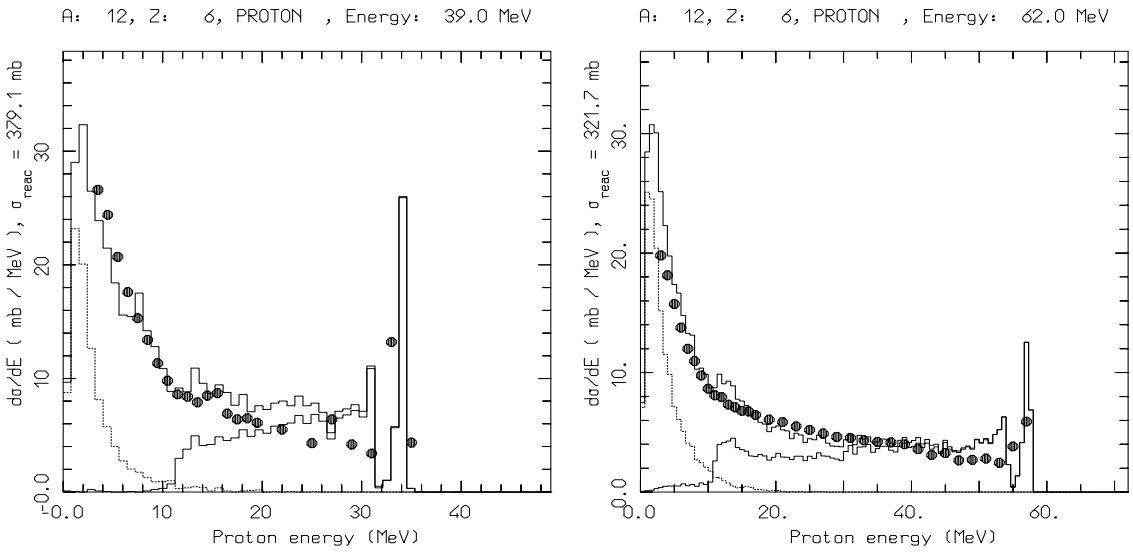

Figure 1: $^{12}C(p,xp)$, at 39 MeV (left) and 62 Mev (right): experimental data(dots) and simulation (thick line). Partial contributions of INC (thin line) and evaporation (dotted line) are shown

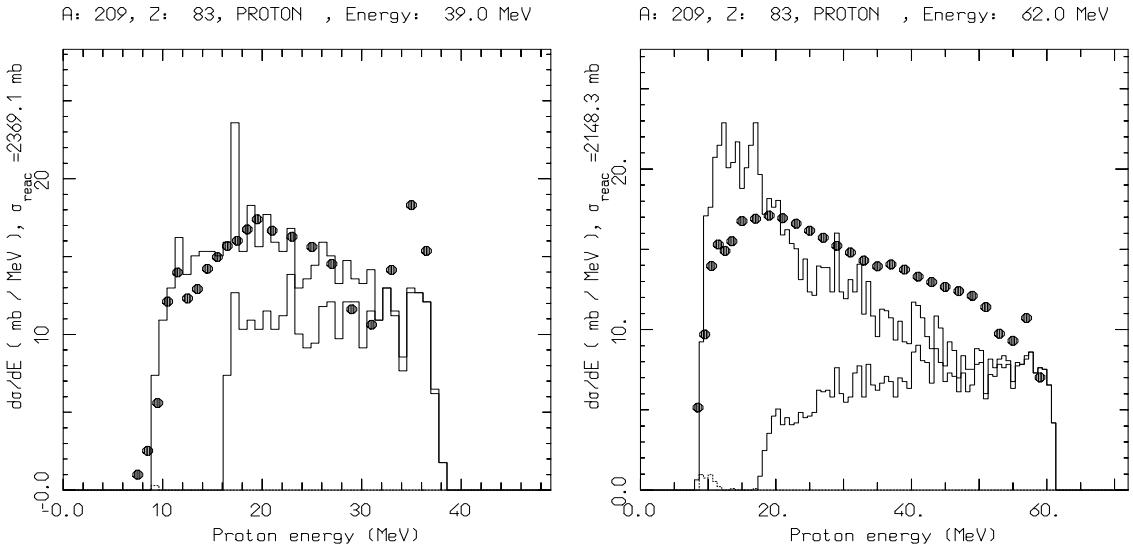

Figure 2: as in fig.1 for $^{209}Bi(p,xp)$, at 39 MeV (left) and 62 Mev (right)

3.2 INC for nucleons

In PEANUT, some intranuclear cascade steps are added on top of the GDH to solve the above mentioned problems. INC is fully performed for proton and neutron projectiles with energy (kinetic) larger than 30 MeV, and for secondaries with energy greater than 50 MeV (calculated in the continuum). Secondaries with 10<E<50 MeV are transported by the INC algorithm till they either escape or reinteract in the nucleus. In the latter case no explicit interaction is performed: only an average Pauli rejection factor[15] is applied and the exciton number is increased. Secondaries with very low energy are directly treated as excitons, but with fixed energy.

The nucleus is modelled as a sphere with density given by a Wood-Saxon shape with standard parameters. It is radially divided in 15 zones of constant density, and its boundary is set at the radius (R_{nuc}) where the density is one hundredth of the central one.

Binding Energies (B.E.) are obtained from mass tables, depending on particle type and on the actual composite nucleus, which may differ from the initial one in the case of multiple particle emission. Relativistic kinematics is applied throughout the cascade, with accurate conservation of energy and momentum. Whenever a particle reaches the emission stage, the recoil energy and momentum of the residual nucleus are calculated and included in the energy balance. It is worth noting that the knowledge of the recoil energy is important in some specific applications, such as radiation damage in semiconductors.

Nucleons (target and projectile) are supposed to move in a radius-dependent well which incorporates both nuclear and Coulomb effects. The nuclear well is presently approximated with a Wood-Saxon shape, but we are also investigating different shapes and a possible dependence on projectile energy

The radial dependence of the potential is discretized in the same intervals as for the nuclear density up to $r = R_{nuc}$, plus three additional intervals in the zone where the nuclear potential goes to zero. For the Coulomb potential, 7 zones have been added to calculate trajectories of outgoing particles up to the radius at which the potential is 1/10 of its value at the barrier, while Coulomb deflection of incoming particles is calculated analytically.

All particles are transported along paths which are subject to curvature in the Coulomb and nuclear potentials. This enhances the probability of peripheral collisions and of backward emission with respect to the conventional straight path approximation.

Path lengths of nucleons in the nucleus are sampled according to the local density and to free nucleon-nucleon cross sections. To take into account the Fermi momentum distribution of nucleons, sampling is performed adopting the maximum possible value of the free cross section in the nucleon-nucleon center of mass (c.m.s.). A target nucleon momentum is then sampled from the Fermi distribution, with random orientation, and the nucleon-nucleon c.m.s. energy is calculated. The ratio

between the free cross section at the actual c.m.s. energy and the maximum cross section gives the appropriate rejection factor to be applied to the collision.

C.m.s. angles after the collision are sampled from experimental differential N-N cross sections. After transformation to the coordinate system of the nucleus at rest, both particle energies are checked to ensure that the Pauli principle is satisfied, i.e. both must be above the Fermi level, otherwise the collision is rejected and a new step is sampled.

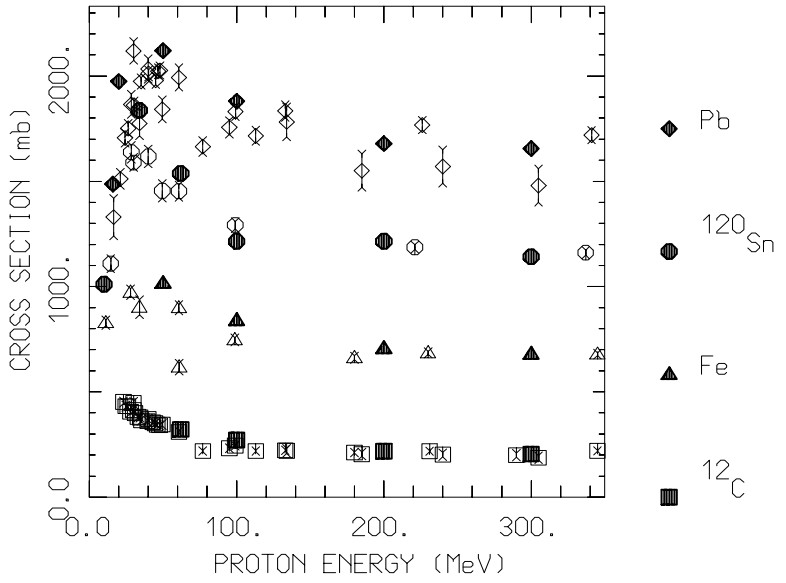

Figure 3: Calculated (black symbols) and experimental (open symbols) proton reaction cross sections

3.3 INC for Pions

The algorithm is essentially the same for pions as for nucleons, only the interaction types and the potential well are different. Of course all secondary nucleons generated in pion interactions are transported or converted into excitons as described above, while pions are followed till they escape or are absorbed. In calculating the pion path length in the nucleus and the interaction kinematics, three processes are taken into account: elastic scattering and charge exchange on single nucleons, and absorption on nucleon pairs. For stopped negative pions also the radiative capture process on single nucleons is considered. The radius where stopped pion absorption takes place is sampled assuming a quadratic dependence of the absorption probability on the nuclear density.

Free elastic and charge exchange cross sections (differential and total) for the three charge states of the pions on both types of nucleons are linked by isospin considerations,[16] an can all be derived from the three experimentally known ones: $\sigma^{+}_{El} = \sigma(\pi^{+} + p \rightarrow \pi^{+} + p)$, $\sigma^{-}_{El} = \sigma(\pi^{-} + p \rightarrow \pi^{-} + p)$, $\sigma^{-}_{CX} = \sigma(\pi^{-} + p \rightarrow \pi^{\circ} + n)$

In deriving the cross sections related to other charge states corrections due

to mass differences have been taken into account (see for instance ref.[17]).

Absorption on nucleon pairs has been divided into s-wave (non-resonant) and p-wave resonant scattering. The s-wave cross section, which is important at low energies, can be calculated from the s-wave absorptive part of the pion-nucleus optical potential[18]:

$$\sigma_A^S(\omega) = \frac{4\pi}{p}(1 + \frac{\omega}{2m})ImB_0(\omega)\rho \tag{1}$$

where ω is the total pion energy and p its momentum in the laboratory frame, and ImB_0 is taken equal to $0.14fm^4$ as in ref..[19] The relative probability of absorption on different nucleon pairs here and in the absorption of stopped pions is left as an adjustable parameter.[20] P-wave resonant absorption is modelled as a two-step process: $\pi + N_1 \rightarrow \Delta$ followed by $\Delta + N_2 \rightarrow N_1' + N_2'$. The analogue process for resonant π-nucleon scattering (or charge exchange) is $\pi + N_1 \rightarrow \Delta$ followed by $\Delta \rightarrow N_1' + \pi'$. In calculating pion absorption, we take for the Δ formation cross section a Breit-Wigner shape fitted on the experimental total πN cross section, as in,[21] and multiply it by the relative absorption width: $Im\Sigma/\frac{\Gamma}{2}$, where Γ is the free Δ width, and $Im\Sigma$ is the absorptive width as given by Oset *et al.*.[22]

The angular distribution of emitted nucleons is taken equal to the $\pi^+ d$ or π^- ^{3}He experimental ones,[23] depending on the target nucleon pair. The choice of the latter is based on isospin considerations.[21]

The potential felt by pions is (somewhat arbitrarily) assumed to have a resonant shape similar to that of the cross section, with a depth of about 100 MeV at resonance. Such a depth was found to be necessary to reproduce the large experimental values of the reaction cross section. Work is in progress to relate it to the standard pion optical potential.

3.4 Angular distributions

The angular distribution of particles emitted in the INC steps is directly derived from two-body kinematics, coordinate transformation to the lab frame and curved path transport.

On the contrary, in the exciton model the angular dependence has to be somehow added, since it is not intrinsic in the formulation. Many different approaches have been developed recently, most of which rely on the fast particle approximation. We follow the formulation of Mantzouranis et al.,[24] as implemented by Akkermans et al..[25] In this model the angular orientation of the nucleus at each step is defined by the direction of the fast particle, which changes gradually in a series of two-body collisions. The transition rate between different exciton states is supposed to be factorizable in an energy-dependent and an angle-dependent factor. The same factorization holds then for the resulting emission probability :

$$\frac{dP_{x,n,\theta}(\epsilon)d\epsilon}{d\Omega} = P_{x,n}(\epsilon)d\epsilon \cdot \sum_l a_l P_l(cos(\theta)) \tag{2}$$

where $P_{x,n}(\epsilon)d\epsilon$ is the angle-integrated emission probability from an n-exciton state as given by GDH.

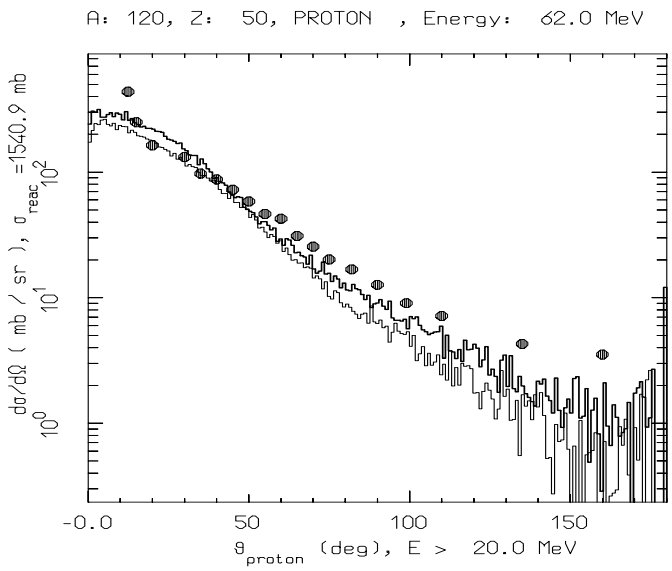

Figure 4: Angular distribution of protons with $E > 20$ MeV following the reaction ^{120}Sn(p,px) at 62 MeV. Dots:experimental data, thick line: PEANUT with curved path, thin line: PEANUT with straight path

Further approximations are introduced in the calculations of the a_l of eq. 2: in the binary collisions the Fermi motion of target nucleons and the Pauli exclusion principle are neglected, as are reflection/refractions at the nuclear surface. Nevertheless, the use of eq. 2 in conjunction with the curved path INC leads to very satisfactory results.

3.5 Evaporation

At the end of the exciton chain, the residual nucleus is a thermally equilibrated system with a certain amount of excitation energy, that can be spent in particle evaporation. The evaporative process is accomplished by a modified version of the EVAP-5 model from the HERMES code.[26] Modifications include different parametrizations of the level density,[27] now tabulated both with A and Z dependence and with the high temperature behaviour suggested by Ignatyuk,[28] and the inclusion of relativistic kinematics.

4. Results

In the following, comparisons between thin-target experimental data and the stand-alone version of PEANUT are presented. Calculations of full cascades in complex geometries performed with FLUKA92 can be found elsewhere.[2,29] In FLUKA92 an earlier version of the algorithm is implemented, without path curvature and pion

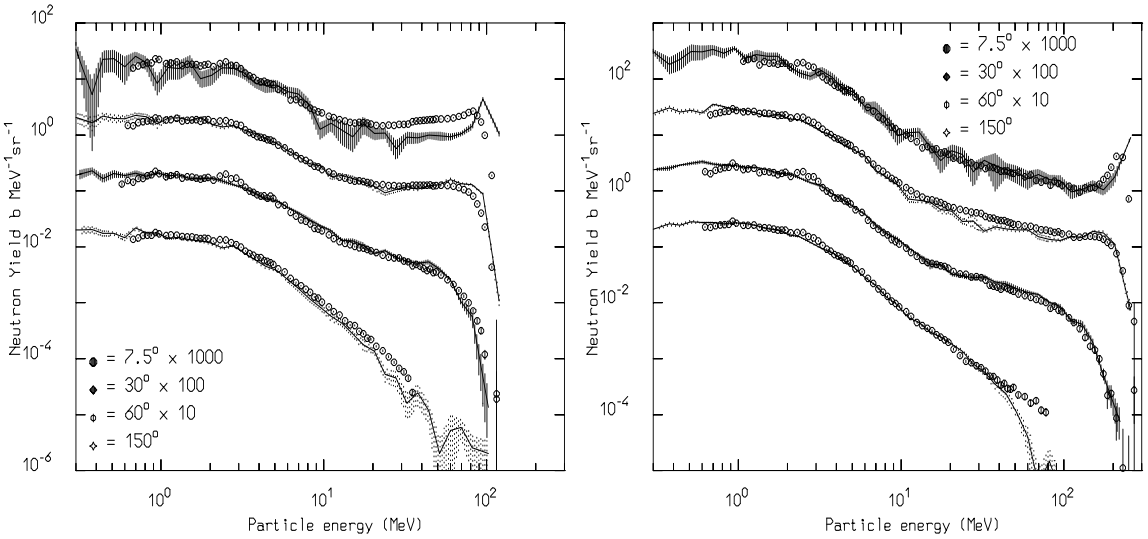

Figure 5: Neutron spectra at different angles following proton bombardment of natural Fe at 113 MeV (left) and natural Pb at 256 MeV (right). Lines with shaded areas are PEANUT calculations with errors, dots are experimental data

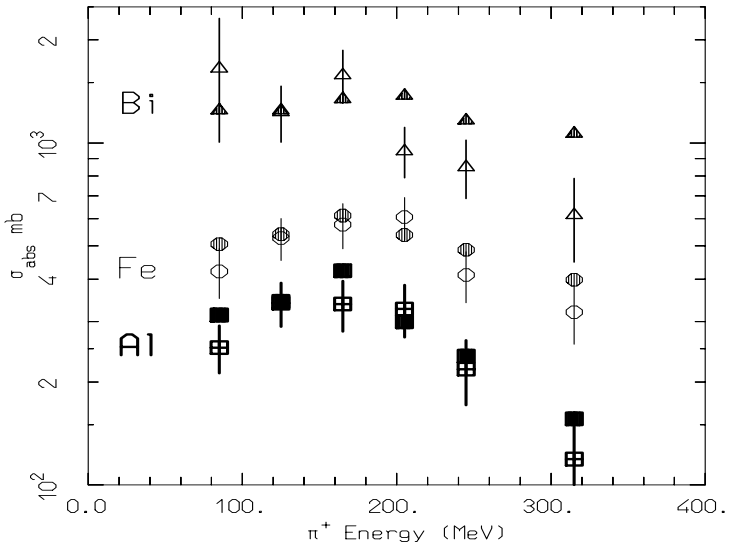

Figure 6: Positive pion absorption cross section vs. pion energy. Open symbols=data, full symbols: PEANUT

transport.

4.1 Benchmarks on nucleon induced reactions

Most available data refer to proton spectra following proton induced reactions

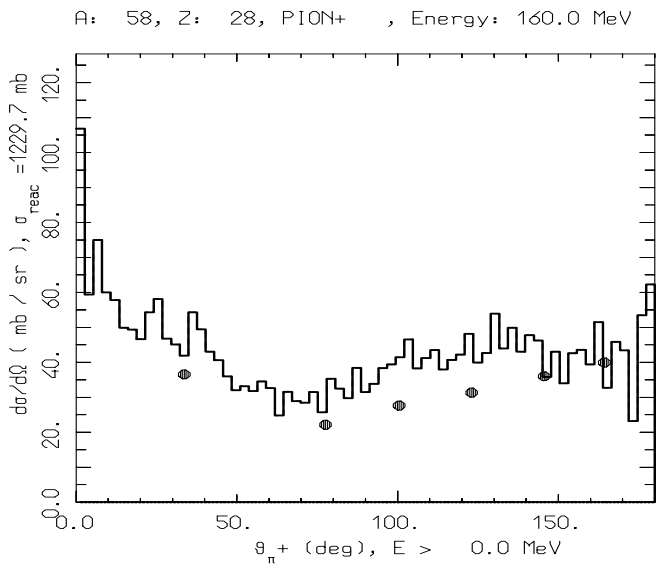

Figure 7: Angular distribution of pions inelastically scattered by a Ni target. Incident energy: 160 MeV . Dots: exp. data, histogram: PEANUT results

at energies lower than 100 MeV. It has to be noticed that many experiments were performed on near-magic nuclei, where shell effect can heavily affect the spectra, expecially for low incident energy.

In figs.1 ,2 two (hopefully) representative spectra are shown, i.e. with a light target (C) at low (39) MeV and medium (62 MeV) energy in fig.1 and a heavy target (Bi) in fig.2 The agreement with data is very satisfactory, not only in the shape, but also in the absolute normalization. It is in fact possible to obtain nucleon-nucleus reaction cross sections from the stand-alone PEANUT (see fig. 3), although in its FLUKA implementation tabulated cross sections obtained from a fit to experimental data are used, mainly to improve speed performances.

Data on angular distributions are from the same sources. Here the effect of the curvature of nuclear trajectories is remarkable, expecially at backward angles, as can be seen from fig.4, where a comparison with the straight path algorithm is presented.

At higher energies, we were able to compare PEANUT results with double differential neutron spectra following bombardment of various targets with 113 and 256 MeV protons.[31,32] Results of the comparison for a natural Fe target at 113 MeV and a natural Pb target at 256 MeV are presented in fig. 5. Again, the agreement between data and calculations is satisfactory.

4.2 Benchmarks on pion-induced reactions

Since the development of this part of the code is still in progress, we did not expect optimal results. As can be seen from tab.1 values of charge exchange

Table 1: Single charge exchange cross sections for 160 MeV pions incident on different targets

Projectile	Target	σ_{CX} (mb)	
		Exp.	PEANUT
π^-	^{12}C	64. ± 10.	66. ± 6.
π^-	^{18}O	73. ± 15.	86. ± 6.
π^-	^{120}Sn	127. ± 25.	151. ± 14.
π^+	Pb	252. ± 30.	251. ± 20.
π^-	Pb	113. ± 16.	181. ± 18.

cross sections on different isotopes[33] are well reproduced, as are absorption cross sections on light nuclei (see fig.6). Conversely, problems are evident from fig.6 in the absorption cross section on heavy nuclei.[34] The angular distribution of scattered pions[35] seems to have the right shape, as can be seen in fig. 7.

5. Conclusions

The proposed algorithm succeeds in reproducing spectra and angular distributions in nucleon induced reaction below 300 MeV. Preliminary results on pion transport are encouraging. Its extension at higher energies should be straightforward with the inclusion of the single pion production process, both in nucleon-nucleon and in pion-nucleon interactions. Work is also in progress to include in PEANUT algorithms describing competing processes, such as high energy fission and nuclear fragmentation.[36]

References

1. P.A. Aarnio, A. Fassò, J.-H. Möhring, J. Ranft and G.R. Stevenson, *Report* **CERN TIS-RP/168** (1986) and **CERN TIS-RP/190** (1987)
2. A. Fassò et. al. *FLUKA92*, presented at the Workshop on Simulating Accelerator Radiation Environments, 11-15 January 1993, Santa Fe
3. K. Hänssgen, H.J. Möhring and J. Ranft, *Nucl. Sci. Eng.* **88** (1984) 552.
4. R. E. Prael and M. Bozoian, *Adaptation of the Multistage Preequilibrium Model for the Monte Carlo Method* **LA-UR-88-3238**, Los Alamos National Laboratory, 1988
5. A. Ferrari, P.R. Sala, A. Fassò and G.R. Stevenson, in *Proc. II int. Conference on Calorimetry in High Energy Physics*, ed. A. Ereditato, (World Scientific, 1992)
6. P.A. Aarnio et al. *FLUKA: Hadronic Benchmarks and Applications*, this Conference.
7. H. W. Bertini, *Phys. Rev.* **131** (1963) 1801.
8. E. Gadioli and P. E. Hodgson, *Pre-equilibrium Nuclear Reactions* (Clarendon Press, Oxford, 1992).

9. J. J. Griffin, *Phys. Rev. Lett.* **17** (1966) 438.
10. H. Feshbach, A. M. Kerman, S. Koonin, *Ann. Phys.* **125** (1975) 429.
11. M. Blann, *Ann. Rev. Nucl. Sci.* **25** (1963) 123.
12. M. Blann, *Phys. Rev. Lett.* **27** (1971) 337.
13. M. Blann, *Phys. Rev. Lett.* **28** (1972) 757.
14. I. Dostrowsky, Z. Fraenkel and G. Friedlander, *Phys. Rev.* **116** (1959) 683.
15. K. Kikuchi and M. Kawai, *Nuclear Matter and Nuclear Interactions* (North-Holland, Amsterdam, 1968)
16. W. O. Lock and D. F. Measday, *Intermediate Energy Nuclear Physics* (Methuen & co, London, 1970).
17. C.J. Joachain, *Quantum Collision Theory* (North-Holland, Amsterdam, 1975)
18. T. Ericson and W. Weise *Pions and Nuclei* (Clarendon Press, Oxford, 1988)
19. L. L. Salcedo et al., *Nucl. Phys.* **A484** (1988) 557.
20. E. Gadioli and E.Gadioli Erba, *Phys. Rev.* **C36** (1987) 741.
21. J. N. Ginocchio, *Phys. Rev.* **C17** (1978) 195.
22. E. Oset and L. L. Salcedo, *Nucl. Phys.* **A468** (1987) 631.
23. H. J. Weyer, *Phys. Rep.* **195** (1990) 295.
24. G. Mantzouranis, D. Agassi, and H. A. Weidenmüller, *Phys. Lett.* **57B** (1975) 220.
25. J. M. Akkermans, H. Gruppelaar and G. Reffo, *Phys. Rev.* **C22** (1980) 73.
26. P. Cloth et al., *HERMES User's Guide* KFA-IRE-E AN/12/88 (1988)
27. R. E. Prael, *private communication*
28. A. V. Ignatyuk, G. N. Smirenkin and A. S. Tishin, *Sov. J. Nucl. Phys.* **21** (1975) 255.
29. A. Fassò et al., *A Comparison of FLUKA simulations with Measurements of Fluence and Dose in Calorimeter Structures*, to be published in Nucl. Instr. Meth. A
30. F. E. Bertrand, R. W. Peelle *Phys. Rev.* **C8** (1973) 1045.
31. M. M. Meier, D. A. Clark, C. A. Goulding, J. B. McClelland, G. L. Morgan and C. E. Moss, *Nucl. Sci. and Eng.* **102** (1989) 310.
32. M. M. Meier, W. B. Amian, C. A. Goulding, G. L. Morgan and C. E. Moss, *Nucl. Sci. and Eng.* **110** (1992) 289.
33. D. Ashery et al. *Phys. Rev* **C30** (1984) 946.
34. D. Ashery et al., *Phys. Rev* **C23** (1981) 2173.
35. S. M. Levenson et al. *Phys. Rev.* **C28** (1983) 326.
36. P. A. Aarnio and M. Huhtinen, *this Conference*